Stability Analysis of Streaks Induced by Optimized Vortex Generators

Connor Klauss*
University of Maryland, College Park, MD 20742, USA

Clark C. Pederson†
NASA Langley Research Center, Hampton, VA 23681, USA

Pedro Paredes‡
National Institute of Aerospace, Hampton, VA 23666, USA

Meelan M. Choudhari§
NASA Langley Research Center, Hampton, VA 23681, USA

Boris Diskin¶
National Institute of Aerospace, Hampton, VA 23666, USA

James D. Baeder ‖
University of Maryland, College Park, MD 20742, USA

Numerical computations are performed to investigate the potential for transition control in an axisymmetric boundary layer via fully realizable, streamwise stationary streaks induced by an azimuthally periodic array of surface mounted vortex generators (VGs). Previous work has shown that suitable streaks of this type can significantly reduce the growth of Mack's second mode instabilities, but large streak amplitudes can make the flow susceptible to previously absent streak instabilities that can become the leading cause of transition. Here, we use the adjoint capabilities of the SU2 flow solver to optimize the VG shape to maximize the reduction in the growth of second-mode disturbances while also preventing the streak amplitudes from reaching large enough values to precipitate an earlier onset of transition via streak instabilities. The geometry and the freestream flow conditions are selected to match a relevant trajectory location from the HIFiRE-1 flight experiment. Results show that the optimized VGs can increase the mean streak amplitude by 117% with respect to a manually developed baseline design. The stability of this optimized basic state is analyzed via the plane-marching parabolized stability equations, predicting a fully laminar flow over the entire cone, or equivalently, yielding transition delay of 130% versus the 17% for the baseline VGs.

Nomenclature

A	=	streak amplitude [m]
h_ξ	=	streamwise metric factor
h_ζ	=	azimuthal metric factor [m]
J	=	objective function
k	=	roughness height [m]
L	=	reference length [m]

*Graduate Student, Department of Aerospace Engineering. Computational AeroSciences Branch, NASA LaRC. AIAA Student Member
†Aerospace Technologist, Aerothermodynamics Branch, NASA LaRC. AIAA Member
‡Senior Research Engineer. AIAA Senior Member
§Aerospace Technologist, Computational AeroSciences Branch. AIAA Fellow
¶Senior Research Fellow. AIAA Associate Fellow
‖Samuel Langley Professor, Department of Aerospace Engineering. AIAA Member

M	=	Mach number
N	=	logarithmic amplification factor
$\bar{\mathbf{q}}$	=	vector of base flow variables
$\tilde{\mathbf{q}}$	=	vector of perturbation variables
$\hat{\mathbf{q}}$	=	vector of amplitude variables
r_b	=	local radius of axisymmetric body at the axial station of interest [m]
t	=	time [s]
(u, v, w)	=	streamwise, wall-normal, and spanwise velocity components [m s^{-1}]
(x, y, z)	=	Cartesian coordinates [m]
α	=	streamwise wavenumber [m^-1]
δ_h	=	boundary layer thickness [m]
λ	=	azimuthal wavelength [rad]
ω	=	disturbance angular frequency [rad s^{-1}]
ρ	=	density [kg m^{-3}]
(ξ, η, ζ)	=	streamwise, wall-normal, and azimuthal coordinates [m, m, -]
Superscripts		
$*$	=	dimensional value
Subscript		
∞	=	freestream value
ST	=	streak
tr	=	transition location

I. Introduction

Laminar-turbulent boundary layer transition plays a significant role in the performance of hypersonic vehicles, causing significant increases in both skin friction and post-transition wall heating. The transition mechanisms must be studied and understood with the potential goal of improving vehicle performance by delaying boundary layer transition.

Under low levels of background disturbances, transition is initiated by an exponential amplification of linearly unstable eigenmodes, i.e., modal instabilities of the laminar boundary layer. In two-dimensional boundary layers over sufficiently smooth aerodynamic surfaces, different mechanisms dominate the exponential growth phase depending on the flight speed. In the incompressible regime, the most amplified disturbances correspond to planar, i.e., two-dimensional, Tollmien-Schlichting (TS) waves, whereas oblique first-mode instabilities are dominant in supersonic boundary layers. Transition in the hypersonic regime is dominated by planar waves of the second mode, i.e., Mack-mode (MM) type [1].

In the presence of sufficiently strong external disturbances in the form of either freestream turbulence (FST) or three-dimensional wall roughness, streamwise streaks involving alternation between low and high regions of streamwise velocity have been observed in incompressible boundary layers [2, 3]. Further research in incompressible flows has shown that streaks with sufficiently high amplitudes can become unstable and initiate shear-layer instabilities that lead to a form of "bypass transition" [4]. When the streak amplitudes are low enough to avoid transition due to streak instabilities (SI), i.e., when the background disturbance level is relatively moderate, the streaks can actually reduce the growth of TS waves in incompressible flows as documented in both theoretical and experimental studies [5–7]. The stabilizing effect of stationary streaks in low-speed boundary layers has been used in passive flow control strategies to demonstrate transition delay via micro vortex generators (VGs) along the body surface [8, 9].

Numerous research efforts have focused on the tripping of hypersonic boundary-layer flows through roughness elements. However, a few experimental and numerical studies have also reported a roughness-related delay in transition under specific circumstances. The latter studies have primarily focused on two-dimensional roughness elements. James [10] considered fin-stabilized hollow tube models in free flight with a screw-thread type of distributed two-dimensional roughness and found that for a given freestream Mach number in the range of 2.8 to 7, there exists an optimum roughness height that yields the largest delay in transition. Fujii [11] studied the effects of two-dimensional roughness by using a 5° half-angle sharp cone at a freestream Mach number of 7.1 and also reported transition delay under certain conditions when the wavelength of the wavy wall roughness was comparable to that of the MM instabilities. More recently, Fong et al. [12, 13] performed numerical and experimental studies, respectively, that were focused on the effect of two-dimensional surface roughness on the stability of a hypersonic boundary layer at a freestream Mach number of 6. The experiments [13], carried out in the Boeing/AFOSR Mach 6 Quiet Tunnel at Purdue University, used a flared cone model with 2D roughness strips and supported the numerical predictions indicating a stabilizing influence of

roughness on the amplification of MM disturbances [12]. In particular, these studies showed that the most dominant MM instability could be suppressed through a judicious placement of the roughness elements on the cone surface.

Additionally, there is limited experimental evidence concerning delayed transition in a hypersonic boundary layer due to three-dimensional roughness elements. Experiments by Holloway and Sterrett [14] in the NASA Langley 20-inch Mach 6 tunnel used a single row of spherical roughness elements that were partially recessed within a flat-plate model. Data for multiple values of the boundary-layer-edge Mach number were obtained by varying the plate mounting angle. These investigators found that, for cases with the smallest roughness diameters, transition was delayed for edge Mach numbers larger than 3.7, which approximately corresponds to the lower bound for second-mode dominance over first-mode instabilities in a flat-plate boundary layer at typical wind tunnel conditions. Therefore, the results are suggestive of a stabilizing influence of roughness-induced streaks on MM waves. Consistent with additional findings by Holloway and Sterrett [14], recent research [15, 16] also established that the same streaks can develop high-frequency instabilities when the roughness height becomes sufficiently large, resulting in an earlier transition relative to that over a smooth surface.

Theoretical studies of the interaction between stationary disturbances and MM instabilities in hypersonic boundary layers were first initiated during the last decade. Li et al. [17] studied the interaction of Görtler vortices with MM instabilities on a flared cone, demonstrating a possible route to transition via this interaction. Li et al. [18] studied the secondary instability of crossflow vortices in the hypersonic boundary layer over a yawed cone and found that nonlinearly saturated crossflow vortices destabilize the Mack modes, which dominate the onset of transition in comparison with the intrinsic secondary instabilities of crossflow vortices, i.e., instability modes that do not originate from the second-mode instability [19, 20]. Ren et al. [21] studied the stabilizing effect of weakly nonlinear suboptimal streaks and Görtler vortices on the planar first-mode and MM instabilities. They documented a slight reduction in the logarithmic amplification N-factor of approximately $\Delta N = 0.2$ relative to the baseline, zero-streaks flat-plate boundary layer. Additional investigations [22–24] related to axisymmetric, hypersonic boundary layers over circular cones in ground test facilities as well as under flow conditions representative of high altitude flight have shown that finite-amplitude optimal growth streaks can substantially reduce the amplification of planar MM instabilities, but also that oblique first-mode waves can be destabilized by morphing into SI instabilities.

In continuing the study of the effects of streamwise streaks on boundary layer, it is important to make note of the difference between optimal streaks and realizable streaks. Optimal streaks are theoretical streaks produced by vortices well above the wall. While these streaks are useful in examining the mechanisms behind boundary layer transition, they are not likely to be found in nature. Because of this, it is important to examine realizable streaks, which are suboptimal streaks that can feasibly be produced by conventional actuation methods such as roughness elements on the wall [25–27]. If the attenuation of modal instabilities in boundary layers is to be achieved, one potential route is through the implementation of these realizable streaks.

We examine the effects of the wake of a periodic array of wall-mounted VGs on the dominant instability waves in axisymmetric or two-dimensional boundary layers at hypersonic Mach numbers. The selected geometry is a 7° half-angle circular cone with $r_n^* = 2.5$ mm nose radius and $L_c^* = 2.0$ m length. The freestream parameters ($M_\infty = 5.3$, $Re_\infty = 13.42 \times 10^6$ m^{-1}, $T_\infty^* = 201.4$ K) are selected to match flow conditions of the HIFiRE-1 flight experiment during the ascent phase at time equal to 21.5 s [28]. The compressible laminar boundary-layer flow is simulated by solving the Navier-Stokes equations. A good correlation between experimental measurements and theoretical predictions based on the parabolized stability equations (PSE) has confirmed that laminar-turbulent transition in this flow is driven by the modal growth of planar MM instabilities [29]. The perturbed three-dimensional boundary layer is used as a basic state for the subsequent modal instability analysis by means of the plane-marching PSE.

This study uses adjoint-based sensitivity analysis to optimize the VG shapes subject to suitable constraints and evaluates the performance improvement resulting from the optimization in the form of delayed boundary layer transition delay at flight conditions. The adjoint capability of Stanford University's open-source CFD solver SU2 was used to design a vortex generator and induce an optimized realizable streak downstream. In that regard, the present work represents a follow-on to the previous study by Pederson et al. [30], who incorporated the necessary capabilities to perform VG optimization into the SU2 flow solver. Preliminary results reported in that paper had shown a moderate improvement in the objective function, equivalent to approximately 20.3% of the baseline value. In this paper, a finer mesh is used for the VG optimization, as a grid sensitivity study showed appreciable differences in the wake between the two meshes. Additionaly, several parameters are varied, including the maximum allowable streak amplitude and the maximum allowable height of the VG deformation. Finally, the changes in disturbance amplification characteristics as a result of the VG optimization are assessed by computing the evolution of the relevant instabilities behind the VGs and comparing them with the N-factor value expected to correlate with the onset of transition. Section II of this paper

provides a brief background on the theory behind the shape optimization and the plane-marching PSE. Subsequently in Section III, we discuss the VG shape and the stability of the corresponding wake. Finally, a summary of the work is presented and conclusions are stated in Section IV.

II. Theory

Here, we discuss the shape optimization and instability analysis used in this study. In what follows, the Cartesian coordinates are represented by (x, y, z). The computational coordinates are defined as an orthogonal body-fitted coordinate system in the cone region, with (ξ, η, ζ) denoting the streamwise, wall-normal, and azimuthal coordinates, respectively, and (u, v, w) representing the corresponding velocity components. The density and temperature are denoted by ρ and T, respectively.

A. Shape Optimization

We begin with a brief overview of the optimization framework developed by Pederson et al. [30]. The shape of the VG is parameterized by a vector of design variables U, with the objective to minimize a defined scalar function J. The solver begins with a baseline geometry and mesh from which the flowfield is computed. The discrete flowfield U computed by the CFD solver is solved on a grid, denoted X, and is dependent on the VG shape α. The objective function J is evaluated for convergence. If the objective function has converged, the optimization cycle is stopped. IF the objective function has not converged, the adjoint-based sensitivities of the objective function to the VG shape parameters are calculated. The VG shape is updated using the computed sensitivities. From there, the forward solve begins and the optimization cycle repeats.

Formally, the CFD grid is a function of the VG shape parameters, the CFD solution is a function of the CFD grid, and the objective function is a function of the CFD solution. These dependencies can be represented as $J = J(U, X(\alpha))$.

The VG shape optimization problem is subject to three constraints. The first constraint is that the CFD solution must satisfy the compressible Navier-Stokes equations, i.e., $R(U, X) = 0$, where R is the vector of CFD residuals. The second of constraint is that the mesh must accomodate the updated VG shape. This constraint is imposed by defining a mapping of the design varibles to the mesh, represented as $\mathcal{M} : \alpha \rightarrow X$. Collectively, the residual and mapping constraints can be represented as:

$$R(U, X) = 0, \tag{1}$$
$$\mathcal{M}(\alpha) = X, \tag{2}$$

The third and final constraint is imposed to ensure that bypass transition does not occur. The following constraint can be writtin as:

$$C(U) \geq 0. \tag{3}$$

In summary, this optimization problem can be defined as:

$$\min_\alpha J(U), \tag{4}$$
$$\text{subject to} \quad R(U, X) = 0, \tag{5}$$
$$\mathcal{M}(\alpha) = X, \tag{6}$$
$$C(U) \geq 0. \tag{7}$$
$$\tag{8}$$

Further details on the optimization process developed preiously for this study can be found in Pederson et al. [30].

The shape modification is made possible through the use of a free-form deformation (FFD) box, where fourth-order B-splines are used to build the new VG shape informed by the adjoint solution. The optimization problem is computed for as many VG design iterations as are necessary for the objective function to be considered converged, namely, when the solver is incapable of increasing the objective function further through additional iterations. This optimization process is driven by the Sequential Least SQuares Programming (SLSQP), which is a local optimization algorithm implemented in SU2. More details on SU2's capabilities can be found in Palacios et al. [31, 32].

For this study, the objective function to be minimized is defined as the integral of the streak amplitude induced by the VGs:

$$J = -\int_{\xi_1}^{\xi_2} A(\xi) d\xi, \tag{9}$$

where ξ_1 and ξ_2 correspond to a location just downstream of the VGs and a location far downstream from the VGs, respectively. The optimization algorithm seeks to find a local minima of the objective function instead of a local maxima, hence the negative sign in front of the integral. The definition of the objective function in Eq. (9) is informed by previous work establishing a positive relationship between a strong downstream streak amplitude and the damping of second-mode instabilities. This sign convention is used in the previous study by Pederson et al. [30]. The streamwise streak amplitude A is calculated as:

$$A(\xi) = \frac{1}{2u_\infty} \max_{\eta}(\max_{\zeta}(u) - \min_{\zeta}(u)). \tag{10}$$

An upper limit is imposed on the streak amplitude as an additional constraint in the optimization process. A VG design which results in a streak amplitude greater than the imposed limit causes a penalty to the objective function and informs the next design iteration. This is done to prevent untethered growth of the streak amplitude, which could lead to premature growth of SI instabilities growing beyond the critical N-factor required for transition and accelerating the onset of transition.

B. Plane-Marching PSE

The linear, plane-marching PSE are used to predict the linear amplification characteristics of both modulated MM waves and the streak instability waves sustained by finite-amplitude streaks induced by the VGs.

The vector of basic-state variables corresponds to $\bar{\mathbf{q}}(\xi, \eta, \zeta) = (\bar{\rho}, \bar{u}, \bar{v}, \bar{w}, \bar{T})^T$ and the vector of perturbation variables is denoted by $\tilde{\mathbf{q}}(\xi, \eta, \zeta, t) = (\tilde{\rho}, \tilde{u}, \tilde{v}, \tilde{w}, Tp)^T$. The curvature metric factors associated with the streamwise and azimuthal curvature, respectively, are defined as

$$h_\xi = 1 + \kappa\eta, \tag{11}$$

$$h_\zeta = r_b + \eta\cos(\theta), \tag{12}$$

where κ denotes the streamwise curvature, r_b is the local radius, and θ is the local half angle along the axisymmetric surface, i.e., $\sin(\theta) = dr_b/d\xi$.

In the plane-marching PSE context, the perturbations to the streak have the form

$$\tilde{\mathbf{q}}(\xi, \eta, \zeta, t) = \hat{\mathbf{q}}(\xi, \eta, \zeta) \exp\left[\mathrm{i}\left(\int_{\xi_0}^{\xi} \alpha(\xi')\, \mathrm{d}\xi' - \omega t\right)\right]. \tag{13}$$

Substituting Eq. (13) into the linearized Navier-Stokes equations and invoking scale separation between the streamwise coordinate and the other two directions to neglect the viscous terms with streamwise derivatives, the PSE are obtained in the form

$$\left(\mathbf{L}_{PSE} + \mathbf{M}_{PSE}\frac{1}{h_\xi}\frac{\partial}{\partial\xi}\right)\hat{\mathbf{q}}(\xi, \zeta) = 0. \tag{14}$$

The initial disturbance profiles for the plane-marching PSE are obtained using a partial-differential-equation (PDE) based two-dimensional eigenvalue problem (EVP).

The onset of laminar-turbulent transition is estimated using the logarithmic amplification ratio, the so-called N-factor, relative to the neutral location ξ_I where the disturbance first becomes unstable,

$$N = -\int_{\xi_I}^{\xi} \alpha_i(\xi')\, \mathrm{d}\xi' + 1/2 \ln\left[\hat{E}(\xi)/\hat{E}(\xi_I)\right]. \tag{15}$$

The energy norm of $\tilde{\mathbf{q}}$ was derived by Chu [33], and used by Mack [34] for linear stability theory, and is defined as

$$E(\xi) = \frac{1}{L_\zeta}\int_\zeta\int_\eta \tilde{\mathbf{q}}(\xi, \eta, \zeta)^H \mathbf{M}\tilde{\mathbf{q}}(\xi, \eta, \zeta)\, h_\xi\, h_\zeta\, \mathrm{d}\eta\, \mathrm{d}\zeta, \tag{16}$$

where the superscript H denotes conjugate transpose, and $\mathbf{M}$ is the energy weight matrix equal to

$$\mathbf{M} = \text{diag}\left[\frac{\bar{T}}{\gamma\bar{\rho}M^2}, \bar{\rho}, \bar{\rho}, \bar{\rho}, \frac{\bar{\rho}}{\gamma(\gamma-1)\bar{T}M^2}\right]. \tag{17}$$

A more detailed description of the PDE-based two-dimensional EVP and plane-marching PSE methodologies are given by Paredes [35], Paredes et al. [36, 37].

III. Results

In this section, we discuss the unperturbed base state solution, as well as the details of the perturbed flow computed with a high-order DNS solver. Subsequently, we discuss the grid refinement study performed in which solutions computed with SU2 are compared to the high-order DNS solution. Finally, the results of the shape optimization and resulting streak amplitudes are compared to the baseline results, and the stability analysis of the wake of the optimized VG is discussed.

A. Unperturbed Boundary-Layer Flow

The basic state, laminar boundary-layer flow over the cone surface is computed by using a second-order accurate algorithm as implemented in the finite-volume cell-centered compressible Navier-Stokes flow solver VULCAN-CFD* [38]. The VULCAN-CFD solution is based on the full Navier-Stokes equations and uses the solver's built-in capability to iteratively adapt the computational grid to the shock. The basic state solution with no VGs present is computed by using the steady-state module of the solver. The geometry is a 7 degree half-angle circular cone with nose radius 2.5 mm and length of 2.0 m. Sutherland's law is assumed for the viscosity, with the Sutherland's constant set equal to 110.4 K. The Prandtl number is 0.72 for air, and the ratio of specific heats γ is equal to 1.4, as the perfect gas model is considered. The freestream conditions are selected to replicate those of the HIFiRE-1 flight experiment at time equal to 21.5 s during the ascent phase [28], i.e., Mach 5.30 flow with a unit Reynolds number of 13.42×10^6 m^{-1}, freestream temperature of $T^*_\infty = 201.4$ K, and a prescribed surface temperature distribution that corresponds to a wall-to-adiabatic temperature ratio of approximately 0.35 over most of the vehicle [29]. Further details of the unperturbed solution are given by Paredes et al. [24]. In what follows, freestream values are used as the reference values for nondimensionalization. The reference length scale is defined as $\delta = \sqrt{L\nu/u_\infty}$, where $L^* = 1.0$ m.

Experimental measurements and theoretical predictions based on PSE have confirmed that laminar-turbulent transition in this flow is driven by the modal growth of planar MM instabilities [29]. To establish the transition behavior in the absence of stationary streak perturbations, the instability of the unperturbed flow was examined by using PSE by Li et al. [29] and Paredes et al. [24]. The onset of laminar-turbulent transition in the unperturbed boundary-layer flow was estimated on the basis of N-factor evolution corresponding to the planar Mack modes computed with the PSE. For the conditions of the experiment [28], transition onset in the unperturbed cone boundary layer was measured to occur near $\xi_{tr}/L = 0.85$. The PSE results of Paredes et al. [24] show that the peak N-factor at the measured transition location corresponds to $N_{tr} = 14.7$, which is first reached by a planar MM disturbance with a frequency of $\omega = 0.603$. Neither planar nor oblique first-mode instabilities were found to be unstable in the present boundary-layer flow because of the low surface temperature relative to the adiabatic temperature.

B. Baseline Design of Vortex Generators

The axisymmetric boundary-layer flow described in subsection III.A is perturbed via an array of roughness elements centered at a selected axial station. The three-dimensional, azimuthally-periodic, laminar boundary-layer flow over the cone surface with arrays of wall-mounted VGs was computed by using a high-order DNS solver. A detailed description of the governing equations and their numerical solution is given by Wu and Martin [39]. The converged inlet solution of the basic-state flow was interpolated to the DNS mesh as a starting point to avoid resolving the leading-edge of the cone. The inviscid fluxes from the governing equations were computed using a seventh-order weighted essentially non-oscillatory finite-difference WENO scheme introduced by Jiang and Shu [40]. The viscous fluxes were discretized using a fourth-order central difference scheme and time integration was performed using a third-order low-storage Runge-Kutta scheme [41].

The baseline design of the roughness array corresponds to azimuthally equispaced pairs of smooth-shaped VGs with elliptical platforms as described by Paredes et al. [42]. The VGs are designed on the basis of the earlier analysis by

*visit `http://vulcan-cfd.larc.nasa.gov` for further information about the VULCAN-CFD solver

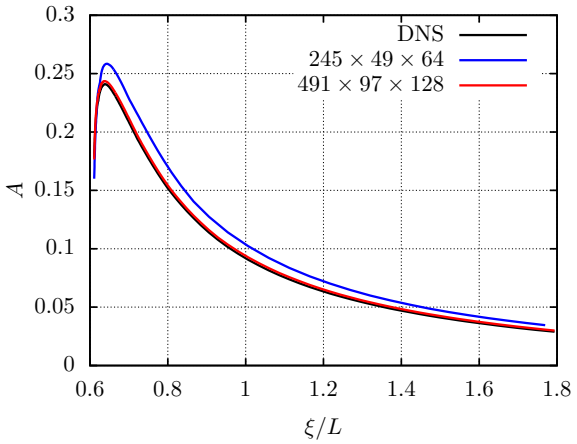

Fig. 1 Evolution of streak amplitudes corresponding to the $245 \times 49 \times 64$ and $491 \times 97 \times 128$ grid solutions with SU2 compared with the $983 \times 192 \times 257$ grid solution from the high-order DNS.

Paredes et al. [24], wherein the interaction between stationary streaks undergoing optimal, nonmodal growth and the MM waves in the present hypersonic boundary-layer flow was analyzed. The VGs are located at $\xi_{VG}/L = 0.6059$, where the N-factor value corresponding to the envelope of MM waves in the unperturbed boundary layer is approximately 2/3 times the N-factor value correlating with the onset of transition, i.e., $N = 2/3N_{tr}$. The azimuthal wavenumber of the VGs is set to 320. The choice of azimuthal wavenumber is consistent with the observation by Paredes et al. [24] that a ratio of wavelength to boundary-layer thickness of $1.4 \leq \lambda_{ST} r_b/\delta_h \leq 2.2$ is highly effective in stabilizing the MM instabilities. For this baseline design of the VGs, Paredes et al. [42] performed the stability analysis of the perturbed flow solution based on the plane-marching PSE and predicted the transition onset to shift downstream from a location of $\xi/L = 0.85$ to $\xi/L = 1$, corresponding to a 17% delay in transition.

The family of computational grids used in the current study are based on the the grid used by Paredes et al. [42]. A grid refinement study is performed in order to determine what level of resolution was required to successfully resolve the streaks. The two meshes are coarsened versions of the DNS mesh used in the study by Paredes et al. [42] with resolutions of $491 \times 97 \times 128$ nodes and $245 \times 49 \times 64$ nodes respectively. As seen in Fig. 1, the $491 \times 97 \times 128$ grid shows good alignment with the high-order DNS solution and follows the general shape of the DNS streak downstream of the VGs. The $245 \times 49 \times 64$ grid solution displays a sharp over approximation of the DNS streak immediately downstream of the VGs, but required nearly an order of magnitude less computational time to converge than the $491 \times 97 \times 128$ mesh. Despite the increased computational time, this study shows that a mesh of resolution $491 \times 97 \times 128$ is refined enough to accurately capture the characteristics of the DNS streak and is used moving forward.

C. Design Optimization of Vortex Generators

SU2's adjoint-based optimization tool is used to determine the optimal VG shape. A variety of cases were run in order to effectively tune the solver, ensure convergence of adjoint solutions, and improve the behavior of the induced streaks. To limit the maximum VG height with respect to the local thickness of the unperturbed boundary layer, an upper limit of 0.4354 mm is imposed on the wall deformation. This limiting value corresponds to a relative VG height of $k/\delta_h = 0.5$, where δ_h refers to the boundary layer height as measured at the VGs location. The boundary layer height was calculated based on a total enthalpy ratio of $h_t/h_{t,\infty} = 0.995$, where the subscript t indicates total enthalpy. Wall deformation is limited to the wall-normal direction for the process of tuning the solver. The objective function is evaluated for each design iteration. The flow and adjoint solutions are considered converged when the residual of the corresponding continuity equations reach values below 10^{-13} and 10^{-8}, respectively. A further reduction of the residual thresholds had no effect on the results. For the adjoint solver, the residual of the continuity equation was last of the five (continuity, momentum, and energy) residuals to reach its convergence value. Thus, by setting the convergence criteria to 10^{-8} it ensured that the other four residuals would be at least an order of magnitude lower and the solution could be considered converged. For the flow solver the opposite was true: the residual of the continuity equation was the first of the five to converge. By requiring the residual to converge to 10^{-13}, it ensured that the other four residuals would reduce to at most 10^{-7}.

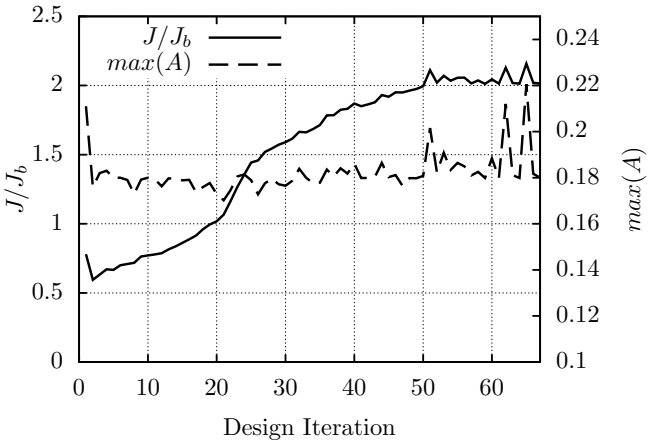

Fig. 2 Objective function and streak amplitude across the design history.

Paredes et al. [24] found that optimal growth streaks become unstable for a maximum streak amplitude greater than $A = 0.2$. The streaks studied in this work however are roughness-induced streaks and, as reported by Denissen and White [43], can become unstable at lower amplitudes than their optimal counterparts. For this reason, an upper limit of $A = 0.18$ was imposed on the VG optimization to ensure that the streaks would not grow to strongly support the amplification of SI instabilities.

Figure 2 displays the objective function and maximum streak amplitude values across the design history. A total of 67 optimization iterations were computed before the optimization process was considered converged. As expected, the maximum streak amplitude from one design iteration to the next oscillates around the imposed value of 0.18. The objective function normalized with the value corresponding to the initial design is increased by over 158% compared to the initial design, and increased by over 100% when compared to the baseline design.

The streamwise evolution of the streak amplitude for the initial and final design iterations are shown in Fig. 3(b) alongside the final VG shape in Fig. 3(a). The optimized streak amplitude evolution begins with a value of approximately 12% immediately behind the VG array and rises rapidly to a maximum of nearly 18% and then remains constant throughout the downstream region. The peak amplitude in this case is somewhat smaller than the relatively sharp peak of approximately 21% in the baseline case, which should reduce the potential for SI instabilities. However, it is the sustenance of the streak amplitude at or just below the imposed upper limit of 18% that should provide a continued reduction in the growth of Mack's second-mode instabilities.

The optimized streak amplitude can be seen with two extrema, the local minimum is attained directly after the VG location and the global maximum is attained further downstream around ξ/L=0.8. Additionally, the downstream amplitude of the streak is much greater and does not decay compared to that of the baseline configuration. Both of these attributes are favorable for mitigating the second-mode instabilities. To better visualize the shape of the VGs in 3D, two renderings of the initial VG shape and the optimized VG shape are shown in Figs. 4(a) and 4(b), respectively.

The instability characteristics of the perturbed, streaky boundary-layer flow are examined next. The plane-marching PSE are used to monitor the evolution of the MM waves, which are modulated by the presence of the azimuthally periodic streaks, and the SI instabilities that can become unstable due to the presence of the streaks and can dominate the process of laminar-turbulent transition. The effect of instability wave scattering by the VGs is not accounted for in the present work. Paredes et al. [24] studied the interaction of oblique and planar MM waves with finite-amplitude optimal streaks and concluded that the planar MM dominates the instability characteristics of both the unperturbed and the perturbed boundary-layer flows, as long as the streak amplitudes are not large enough for the SI sustained by those streaks to cause transition onset. Paredes et al. [24] have also observed that the subharmonic, sinuous mode SI is the most unstable mode for moderate streak amplitudes and, therefore, has the potential to play an important role during the transition process. Based on those findings, the growth of nominally planar MM waves and subharmonic, sinuous SI modes are analyzed next.

Figure 5(a) shows the Mach contours at selected stations within the wake, indicating approximately sinusoidal streaks throughout the length of the computational domain. Figure 5(b) displays the MM and SI growth characteristics of the wake of the optimized VGs with $\max(A) < 0.18$. It can be seen that initially unstable second-mode instabilities decrease rapidly once they encounter the VGs. Furthermore, neither the second-mode instabilities or SI instabilities

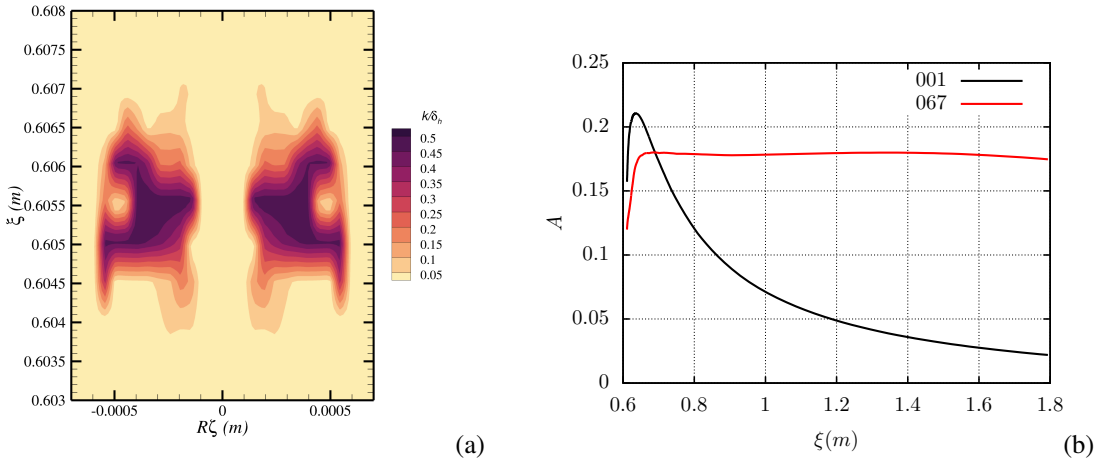

Fig. 3 (a) Top-down view of the optimized VG design for an imposed upper limit of 0.18 on the streak amplitude, colored by normalized distance above the wall. (b) Streak amplitude of the initial shape (black) and optimized (red) vortex generators.

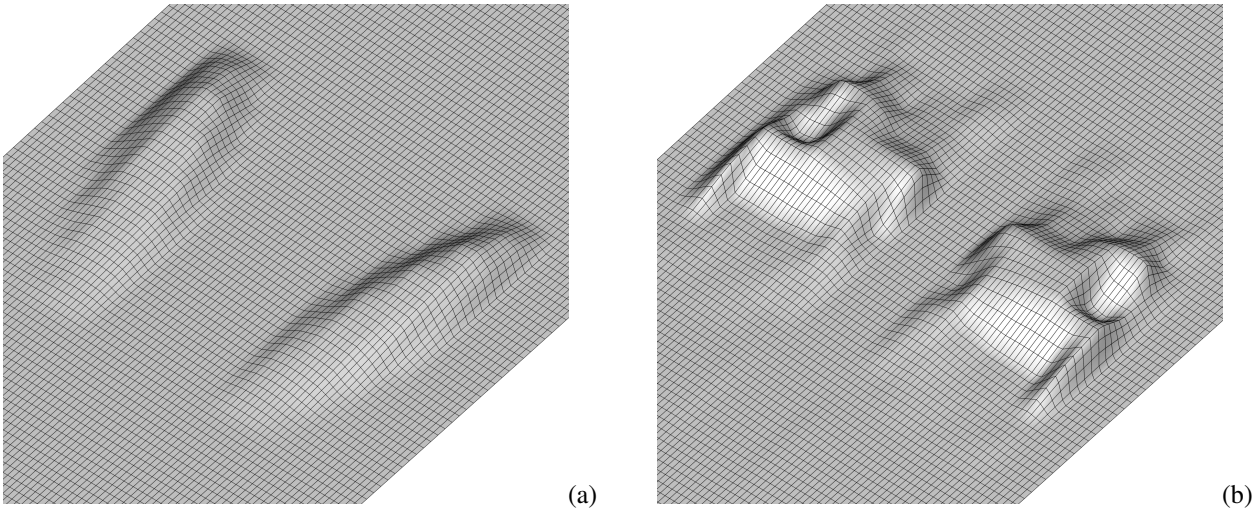

Fig. 4 Zoomed perspective images of the initial VGs (a) and the optimized VGs with an upper limit of 0.18 imposed on streak amplitude (b). Note that the axes ratios have been changed to give a better view of the VG shape.

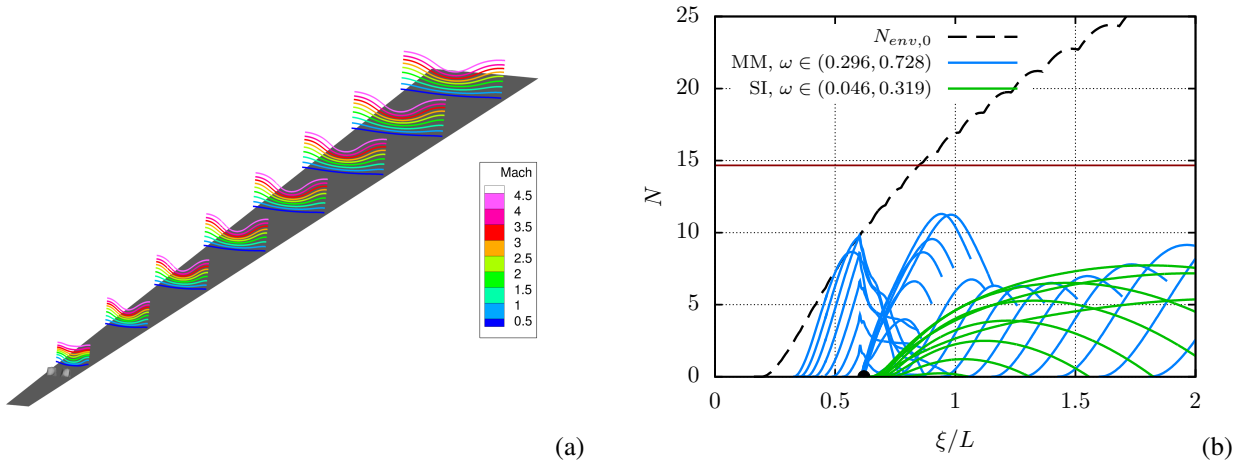

Fig. 5 (a) Mach contours of the wake produced by an optimized VG with an imposed upper limit of 0.18 on the streak amplitude. (b) N-factor curves for planar MM disturbances (MM) and sinuous, subharmonic streak instability modes (SI) for case I with one array of VGs at $\xi_{VG}/L = 0.6059$. The relevant frequency ranges are selected for each disturbance. The dark-red horizontal line denotes the transition N-factor.

reach the critical N-factor of 14.7, which correlated with transition onset due to second mode growth during the HIFiRE-1 flight experiment. The MM instabilities attain a maximum N-factor of nearly 12 in the case of the optimized VGs; therefore, even if transition onset in the presence of streaks were to occur at a reduced critical N-factor of 12 (as against 14.7 in the absence of any streaks) because of a potentially adverse impact of the streaks on the receptivity and the nonlinear breakdown stages, one would still expect the boundary layer to remain laminar throughout the length of the computational domain of up to $x = 2.0$ m. The maximum N-factor attained by the SI modes of instability is approximately 8.

We next demonstrate that the optimal VG configuration from Fig. 4(b) also provides a useful starting point for further design modifications. For example, the onset of transition due to SI instabilities cannot be predicted with a great degree of confidence at present. Choudhari et al. [44] had analyzed the growth of SI instabilities near the centerline of the HIFiRE-5 elliptic cone model and found an N-factor of approximately 15 at the transition location inferred from the flight data. However, because that analysis was limited to a single point along the trajectory, the uncertainty in the resulting correlation is rather high. As a conservative measure to guard against potential transition due to SI instabilities, one could reduce the upper limit imposed on the maximum streak amplitude from 0.18 to 0.16. The results of this case are seen in Fig. 5. The final design of the 0.18 case was used as an initial shape for the optimization, instead of the baseline geometry seen in Fig. 4. The solver took 13 design iterations to decrease the maximum streak amplitude to 0.16, a sharp decrease from the 67 iterations required to get from the baseline design to the desired streak amplitude of 0.18. The new shape of the VGs (Fig. 6(a)) is very similar to that in Fig. 3(a) with the higher limit on the streak amplitude. Furthermore, the resulting evolution of the streak amplitude (Fig. 6(b)) is also very similar to that with $max(A) = 0.18$. The Mach number contours in the wake and the N-factor curves for the MM and SI instability modes are shown in Figs. 7(a) and 7(b), respectively. Whereas the peak N-factor and the corresponding streamwise station for the MM mode amplification is nearly unchanged, the peak N-factor for the SI modes is reduced from 8 to below 5. Again, the flow is predicted to remain laminar throughout the length of the computational domain. This exercise highlights the utility of the design optimization process for developing not only an optimal VG shape for assumed N-factor correlations, but also to define multiple candidate geometries that could be tested in a validation experiment.

IV. Summary and Concluding Remarks

It is known from previous work that suitably tailored, stationary longitudinal streaks excited via surface mounted vortex generators (VGs) can mitigate the growth of Mack's second-mode instabilities in a hypersonic boundary layer without allowing the extraneous SI instabilities to take over as the dominant cause for transition. The efficacy with which realizable streaks in hypersonic boundary layer flow can suppress second-mode instabilities was investigated in

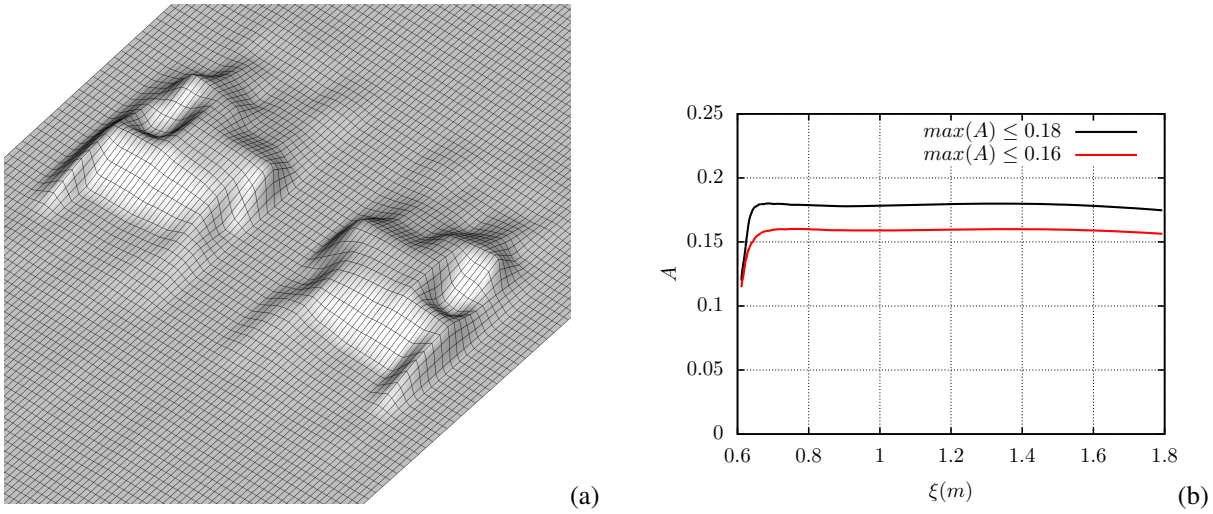

Fig. 6 (a) Zoomed perspective of the optimized VGs with an upper limit of 0.16 imposed on the streak amplitude. Note the axes ratios have been changed to give a better view of the VG shape. (b) Streak amplitude of the initial shape (black) and optimized (red) vortex generators.

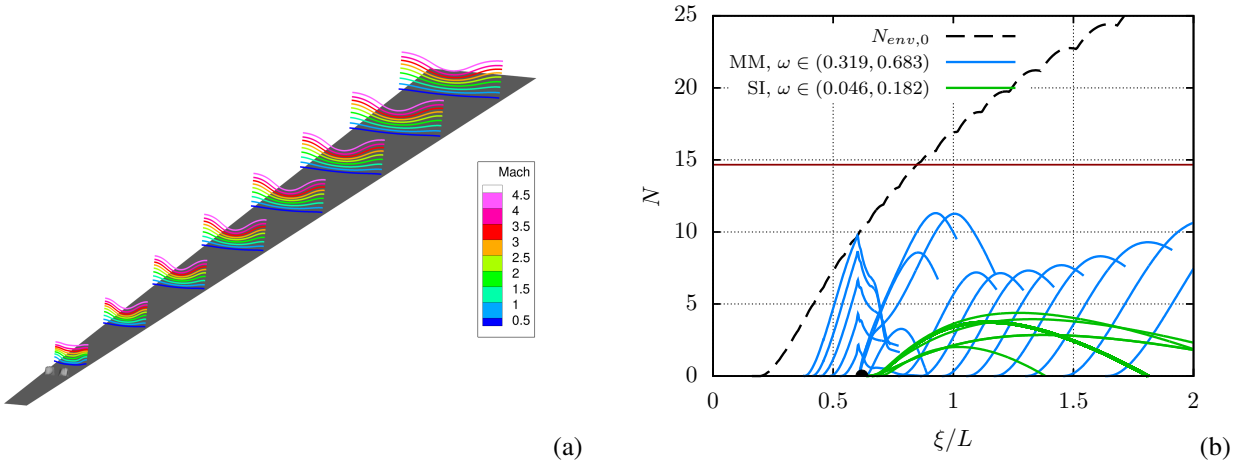

Fig. 7 (a) Mach contours of the wake produced by an optimized VG with an imposed upper limit of 0.16 on the streak amplitude. (b) N-factor curves for planar MM disturbances and sinuous, subharmonic streak instability modes (SI) for case I with one array of VGs at $\xi_{VG}/L = 0.6059$. The relevant frequency ranges are selected for each disturbance. The dark-red horizontal line denotes the transition N-factor.

this paper using adjoint-based optimization of the VG pattern in an axisymmetric, hypersonic boundary layer at cold wall conditions that are representative of high-altitude flight. Previous work had demonstrated that a nonoptimized baseline design consisting of an azimuthal spacing derived from the optimal-transient-growth theory and a manually crafted VG shape could delay the onset of boundary layer transition by approximately 17% for a selected trajectory point from the HIFiRE-1 flight experiment. Preliminary optimization work by Pederson et al. [30] saw a 20.3% increase in the mean streak amplitude from the first to final design. The follow-on work described in the present study reports an increase in the mean streak amplitude by over 158% in the course of the design history when comparing the first and final designs, and an increase in over 100% when comparing the final design to the baseline design. According to the research described in this study, optimized VGs could potentially delay the onset of transition via realizable streaks by up to 130%, making the boundary layer flow over the whole payload surface (up to an extended length of 2 meters) entirely laminar. The peak amplitude was limited to a predetermined value based on previous experience to prevent SI instabilities. The numerical studies reported here, on the other hand, suggests that significant transition delay may be achievable for a range of maximum streak amplitude values. The initial VG design restricted the surface deformation associated with the VGs to positive values, i.e., to a protuberance-only shape that can be achieved without removing any material from the baseline geometry. Future studies should seek to examine the impact on transition delay of VGs allowing for both positive and negative surface deformations, as well as the physical mechanisms behind the interactions of the streaks and the second-mode instabilities.

Acknowledgments

This material is based on work supported by the Air Force Office of Scientific Research under award number FA9550-20-0023 with P.O. Dr. Sarah Popkin as well as the NASA Hypersonic Technology Project (HTP) under the Aeronautics Research Mission Directorate (ARMD). Resources supporting this work are provided by the Department of Defense (DOD) High Performance Computing Modernization Program (HPCMP), the NASA High-End Computing (HEC) Program through the NASA Advanced Supercomputing (NAS) Division at Ames Research Center, as well as the NASA Midrange K cluster at the Langley Research Center.

References

[1] Mack, L., "Boundary Layer Linear Stability Theory," *AGARD–R–709. Special Course on Stability and Transition of Laminar Flow*, 1984, pp. 3.1–3.81.

[2] Klebanoff, P., "Effect of Free-Stream Turbulence on the Laminar Boundary Layer," *Bull. Am. Phys. Soc.*, **16**, 1323, 1971.

[3] Vermeersch, O., and Arnal, D., "Klebanoff-Mode Modeling and Bypass-Transition Prediction," *AIAA J.*, Vol. 48, No. 11, 2010, pp. 2491–2500.

[4] Andersson, P., Brandt, L., Bottaro, A., and Henningson, D., "On the Breakdown of Boundary Layer Streaks," *J. Fluid Mech.*, Vol. 428, 2001, pp. 29–60.

[5] Boiko, A., Westin, K., Klingmann, B., Kozlov, V., and Alfredsson, P., "Experiments in a Boundary Layer Subjected to Free Stream Turbulence. PART 2. The Role of TS-Waves in the Transition Process," *J. Fluid Mech.*, Vol. 281, 1994, pp. 219–245.

[6] Cossu, C., and Brandt, L., "Stabilization of Tollmien-Schlichting Waves by Finite Amplitude Optimal Streaks in the Blasius Boundary Layer," *Phys. Fluids*, Vol. 14, No. 8, 2002, pp. L57–L60.

[7] Bagheri, S., and Hanifi, A., "The Stabilizing Effect of Streaks on Tollmien-Schlichting and Oblique Waves: A Parametric Study," *Phys. Fluids*, Vol. 19, 2007, pp. 078103–1–078103–4.

[8] Fransson, J., Talamelli, A., Brandt, L., and Cossu, C., "Delaying Transition to Turbulence by a Passive Mechanism," *Phys. Rev. Lett.*, Vol. 96, 2006, p. 064501.

[9] Shahinfar, S., Sattarzadeh, S., Fransson, J., and Talamelli, A., "Revival of Classical Vortex Generators Now for Transition Delay," *Phys. Rev. Lett.*, Vol. 109, 2012, p. 074501.

[10] James, C., "Boundary-Layer Transition on Hollow Cylinders in Supersonic Free Flight as Affected by Mach Number and a Screwthread Type of Surface Roughness," NASA TR-Memo-1-20-59A, 1959.

[11] Fujii, K., "Experiment of the Two-Dimensional Roughness Effect of Hypersonic Boundary-Layer Transition," *J. Spacecraft Rockets*, Vol. 43, No. 4, 2006, pp. 731–738.

[12] Fong, K., Wang, X., and Zhong, X., "Numerical Simulation of Roughness Effect on the Stability of a Hypersonic Boundary Layer," *Compt. Fluids*, Vol. 96, 2014, pp. 350–367.

[13] Fong, K., Wang, X., Huang, Y., Zhong, X., McKiernan, G., Fisher, R., and Schneider, S., "Second Mode Suppression in Hypersonic Boundary Layer by Roughness: Design and Experiments," *AIAA J.*, Vol. 53, No. 10, 2015, pp. 3138–3143.

[14] Holloway, P., and Sterrett, J., "Effect of Controlled Surface Roughness on Boundary-Layer Transition and Heat Transfer at Mach Number of 4.8 and 6.0," NASA TR-D-2054, 1964.

[15] Choudhari, M., Li, F., and Edwards, J., "Stability Analysis of Roughness Array Wake in a High-Speed Boundary Layer," AIAA Paper 2009-0170, 2009.

[16] Paredes, P., De Tullio, N., Sandham, N. D., and Theofilis, V., "Instability Study of the Wake Behind a Discrete Roughness Element in a Hypersonic Boundary Layer," *Instability and control of massively separated flows*, edited by V. Theofilis and J. Soria, Springer International Publishing, 2015, pp. 91–96.

[17] Li, F., Choudhari, M., Chang, C.-L., Greene, P., and Wu, M., "Development and Breakdown of Görtler Vortices in High Speed Boundary Layers," AIAA Paper 2010-0705, 2010.

[18] Li, F., Choudhari, M., Paredes, P., and Duan, L., "Secondary Instability of Stationary Crossflow Vortices in Mach 6 Boundary Layer over a Circular Cone," NASA TM-2015-218997, 2015.

[19] Choudhari, M., Li, F., Paredes, P., and Duan, L., "Computations of Crossflow Instability in Hypersonic Boundary Layers," AIAA Paper 2017-4300, 2017.

[20] Choudhari, M., Li, F., Paredes, P., and Duan, L., "Nonlinear Evolution and Breakdown of Azimuthally Compact Crossflow Vortex Pattern over a Yawed Cone," AIAA Paper 2018-1823, 2018.

[21] Ren, J., Fu, S., and Hanifi, A., "Stabilization of the Hypersonic Boundary Layer by Finite-Amplitude Streaks," *Phys. Fluids*, Vol. 28, 2016, pp. 024110–1–16.

[22] Paredes, P., Choudhari, M., and Li, F., "Transition Delay in Hypersonic Boundary Layers via Optimal Perturbations," NASA TM-2016-219210, 2016.

[23] Paredes, P., Choudhari, M., and Li, F., "Stabilization of Hypersonic Boundary Layers by Linear and Nonlinear Optimal Perturbations," AIAA Paper 2017-3634, 2017.

[24] Paredes, P., Choudhari, M., and Li, F., "Instability Wave-Streak Interactions in a High Mach Number Boundary Layer at Flight Conditions," *J. Fluid Mech.*, Vol. 858, 2019, pp. 474–499.

[25] Choudhari, M., and Fischer, P., "Roughness Induced Transient Growth," AIAA Paper 2005-4765, 2005.

[26] Fischer, P., and Choudhari, M., "Numerical Simulation of Roughness-Induced Transient Growth in a Laminar Boundary Layer," AIAA Paper 2004-2539, 2004.

[27] Fransson, J., Brandt, L., Talamelli, A., and Cossu, C., "Experimental and Theoretical Investigation of the Non-Modal Growth of Steady Streaks in a Flat Plate Boundary Layer," *Phys. Fluids*, Vol. 16, No. 10, 2004, pp. 3627–3638.

[28] Kimmel, R., Adamczak, D., Paull, A., Paull, R., Shannon, J., Pietsch, R., Frost, M., and Alesi, H., "HIFiRE-1 Ascent-Phase Boundary-Layer Transition," *J. Spacecraft Rockets*, Vol. 52, No. 1, 2015, pp. 217–230.

[29] Li, F., Choudhari, M., Chang, C., Kimmel, R., Adamczak, D., and Smith, M., "Transition Analysis for the Ascent Phase of HIFiRE-1 Flight Experiment," *J. Spacecraft Rockets*, Vol. 52, No. 5, 2015, pp. 1283–1293.

[30] Pederson, C., Choudhari, M., Zhou, B., Paredes, P., and Diskin, B., "Shape Optimization of Vortex Generators to Control Mack Mode Amplification," AIAA Paper 2020-2963, 2020.

[31] Palacios, F., Alonso, J., Duriasamy, K., Colonno, M., Hicken, J., Aranake, A., Campos, A., Copeland, S., Economon, T., Lonkar, A., Lukaczyk, T., , and Taylor, T., "Stanford University Unstructured (SU2): An Open-Source Integrated Computational Environment for Multi-Physics Simulation and Design," AIAA paper 2013-287, 2013.

[32] Palacios, F., Economon, T. D., Aranake, A., Copeland, S. R., Lonkar, A. K., Lukaczyk, T. W., Manosalvas, D. E., Naik, K., Padron, S., Tracey, B., Variyar, A., and Alonso, J. J., "Stanford University Unstructured (SU2): Analysis and Design Technology for Turbulent Flows," AIAA paper 2014-0243, 2014.

[33] Chu, B.-T., "On the Energy Transfer to Small Disturbances in Fluid Flow (PART I)," *Acta Mechanica*, Vol. 1, No. 3, 1956, pp. 215–234.

[34] Mack, L. M., "Boundary Layer Stability Theory," Tech. Rep. 900-277, Jet Propulsion Lab., Pasadena, CA, 1969.

[35] Paredes, P., "Advances in Global Instability Computations: from Incompressible to Hypersonic Flow," Ph.D. thesis, Universidad Politécnica de Madrid, 2014.

[36] Paredes, P., Hanifi, A., Theofilis, V., and Henningson, D., "The Nonlinear PSE-3D Concept for Transition Prediction in Flows With a Single Slowly-Varying Spatial Direction," *Procedia IUTAM*, Vol. 14C, 2015, pp. 35–44.

[37] Paredes, P., Choudhari, M., and Li, F., "Instaiblity Wave-Streak Interactions in a Supersonic Boundary Layer," *J. Fluid Mech.*, Vol. 831, 2017, pp. 524–553.

[38] Litton, D., Edwards, J., and White, J., "Algorithmic Enhancements to the VULCAN Navier-Stokes Solver," AIAA Paper 2003-3979, 2003.

[39] Wu, M., and Martin, M., "Direct Numerical Simulation of Supersonic Boundary Layer over a Compression Ramp," *AIAA J.*, Vol. 45, No. 4, 2007, pp. 879–889.

[40] Jiang, G., and Shu, C., "Efficient Implementation of Weighted ENO Schemes," *J. Comp. Phys.*, Vol. 126, No. 1, 1996, pp. 202–228.

[41] Williamson, J., "Low-Storage Runge-Kutta Schemes," *J. Comp. Phys.*, Vol. 35, No. 1, 1980, pp. 48–56.

[42] Paredes, P., Choudhari, M., and Li, F., "Transition Delay via Vortex Generators in a Hypersonic Boundary Layer at Flight Conditions," AIAA Paper 2018-3634, 2018.

[43] Denissen, N., and White, E., "Secondary Instability of Roughness-Induced Transient Growth," *Phys. Fluids*, Vol. 25(11), 2013, p. 114108.

[44] Choudhari, M., Li, F., and Paredes, P., "Streak Instabilities on HIFiRE-5 Elliptic Cone," AIAA Paper 2020-0828, 2020.